RSC Advances

ROYAL SOCIETY OF CHEMISTRY

www.rsc.org/advances

Journal Name

RSCPublishing

COMMUNICATION

N-doped ordered mesoporous carbon as high performance anode materials in sodium ion batteries at room temperature

Cite this: DOI: 10.1039/xoxxoooooox

Received ooth January 2012,
Accepted ooth January 2012

DOI: 10.1039/xoxxoooooox

www.rsc.org/

Zhiguang Wang[a], Yueming Li*[a], and Xiao-Jun Lv*[b]

Here we report the electrochemical performance of N-doped ordered mesoporous carbon as anode in sodium ion batteries for the first time. The experiments show that highly reversible capacities as well as good rate performance can be achieved at room temperature; indicating promising future for ordered mesoporous carbon in Na-ion batteries.

Introduction:

Lithium-ion batteries (LIB) have become the dominant storage device for portable appliance since 1990. However, the limited and expensive lithium resources have become a key issue which may limit the future application of LIB. These concerns have led to the active search for suitable alternatives.[1] Sodium ion batteries (SIB) have been given extensive attention due to the abundance and low costs of sodium resources. [2] However, the researches on electrode materials for SIB are rather limited compared to that for LIB until recent years. As is well-known, the electrode materials played critical role in determining the electrochemical performance in batteries. Up to now, the major challenge for SIB is in finding the electrode materials with satisfying electrochemical performance. A lot of materials have been studied as anode candidates in recent years, including titanates,[3, 4] Sn[5, 6] and Sb[7] etc. However, the electrochemical performances of these non-carbonaceous materials as anode in SIB is still far below the actual requirement due to the low capacity or volume expansion during charge/discharge.[8]

Graphite, the common anode material in LIB, has a poor electrochemical performance in SIB because of the weak chemical bonding between graphene and sodium ions. [9, 10] Several types of non-graphitic carbon materials including hard carbons,[11] the defective graphene or B-doped graphene,[12, 13] carbon nanofiber [14] and three dimensional carbon nanosheets framework[15] have shown much improved electrochemical performance in SIB according to the experiments or theoretical predications. Although huge progresses in electrochemical performance have been made for these materials, it appears to be still a bit far away from the practical application at room temperature. Thus novel carbon materials should be developed in order to make continuous progress for SIB. Wenzel *et al* found that non-ordered porous carbons have shown improved kinetics and capacity at room temperature due to the hierarchical structure containing both mesopores and macropores.[16]

The ordered mesoporous materials (OMCs) present many advantages with respect to non-porous or non-ordered materials due to the uniform pore width and large surface area, which facilitate the contact between electrolyte and electrode materials in batteries.[17] In fact, OMCs have attracted a lot of interests due to their large surface area, uniform and adjustable mesopores, chemical stability as well as good conductivity. And studies have shown that OMCs have exhibited an excellent performance in the field of LIB.[18, 19] Furthermore, it has been proven that the doping of heteroatoms such as nitrogen into carbon lattice can greatly enhance the electrochemical performance,[20-25] especially in conductivity and capacity based on our recent work.[26] Considering the similarity between LIB and SIB, it is reasonable to apply the N-doped OMCs as anode material for SIB.

To the best of our knowledge there is no reports on OMCs as anode in SIB up to now, herein, we reported the electrochemical performance of N-doped OMC as anode in SIB. The electrochemical experiments indicated that not only large reversible capacity but also good rate performance can be achieved for N-doped OMC at room temperature.

Experimental

Preparation of N-doped OMC

Mesoporous silica (SBA-15) as template was prepared using the triblock copolymer ($EO_{20}PO_{70}EO_{20}$ (P123, Aldrich)) according to a literature procedure. [27] The typical procedure to prepare ordered mesoporous carbon (CMK-3) is as follow. First, 1.2 g sucrose was dissolved in 5 mL deionized water. Then 1 g SBA-15 and 0.1 mL concentrated H_2SO_4 were added into the mixture under stirring. Thereafter the mixture was dried at 100 °C for 6 h and then heated at 160 °C for another 6h. The as-obtained silica/sucrose mixture (denoted as SSM) was heated to 900 °C under argon atmosphere for 2 h. To get CMK-3, the mixture was immersed into HF aqueous solution to remove silica, filtered with deionized water and dried at 80 °C overnight. To get N-doped OMC, SSM was mixed with urea in mass ratio of 1:1 and heated at 900 °C for 2 h, then the mixture was treated with a similar way to get CMK-3. The nitrogen doped OMC is denoted as NCMK.

Characterization:

The powder X-ray diffraction (XRD) measurements of the samples were recorded on a D-max 2500 X-ray powder diffractometer using a graphite monochromator with Cu Kα radiation (λ = 1.5406 Å). The data were collected between scattering angles (2θ) of 5–80° and 0.7–3° at a scanning rate of 4°/min and 0.2°/min for wide and low angle, respectively. Scanning electronic microscopy was carried out on field emission-scanning electron microscope (FE–SEM, Hitachi-4800S). TEM specimens were prepared by drop–casting the as prepared sample dispersions onto carbon-coated TEM grids and dried in air. A JEM 2010 transition electronic microscopy was used for TEM analysis. X–ray photoelectron spectrum was carried out on ESCALAB 250Xi.

Electrochemical performance

To evaluate electrochemical performance as anode material in Na-ion batteries, the electrodes were constructed according to previous reference.[18] The cells were assembled inside the argon-filled glove box (Braun, H_2O < 1ppm and O_2 < 1ppm) using a sodium metal foil as the counter electrode and the reference electrode, and microporous polypropylene as the separator. The electrolyte used was 1 M $NaClO_4$ in a 1:1 volume ratio ethylene carbonate (EC): dimethyl carbonate (DMC) solvent. Assembled cells were tested on a BT 2000 battery testing unit (Arbin, USA). Galvanostatic charge and discharge of the assembled cells were performed at varied current density between voltage limits of 0.005 to 2.0 V (vs. Na/Na^+). The cyclic voltammetry (CV) measurements were carried out in the potential range of 0.005 to 2.0 V (vs Na/Na^+) on an electrochemical workstation (P4000, Princeton applied research, USA) at room temperature.

Results and discussion:

Morphologies of as prepared NCMK and CMK-3 were observed via high resolution SEM and TEM. As shown in **Fig. 1**A and B, the image of CMK-3 viewed along hexagonal pore direction clearly demonstrated the ordered pores parallel to each other with uniform size of about 5–9 nm. As shown in **Fig. 1**C and 1D, the morphology of NCMK is similar to that of CMK-3 in general, however the ordered degree of NCMK decrease slightly compared with that of CMK-3, which might be related to the urea decomposition in preparation process.

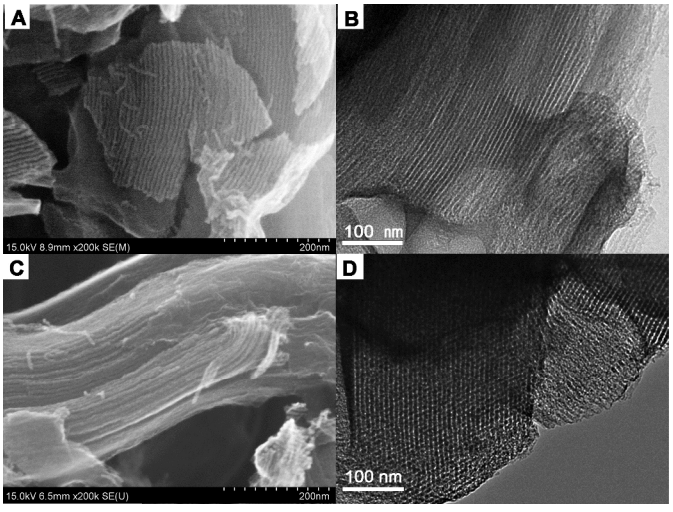

Fig. 1. SEM (A) and TEM (B) images of CMK-3; SEM (C) and TEM (D) images of NCMK.

High resolution TEM of CMK-3 (**Fig. S1**A) shows the partial amorphous characteristic (amorphous with local medium-range order). The local structure of NCMK became much more disordered compared to that of CMK-3, indicating the local structure became more "amorphous" during N-doping process, shown in **Fig. S**1B.

Low and wide angle XRD tests were carried out to determine the internal structure of as prepared samples. The wide angle XRD patterns of CMK-3 and NCMK disclose carbon nature with the low crystalline degree, shown in Fig. 2A. The low angle XRD patterns of CMK-3 sample (Fig. 2B) shows an intense diffraction peak (corresponding to (100)) and two weak peaks (corresponding to (110) and (200)), which are characteristic of two-dimensional hexagonal structure of mesoporous materials. The N-doped sample shows a similar pattern to that of CMK-3, indicating the pore structure retained after urea treating, consistent to the SEM results.

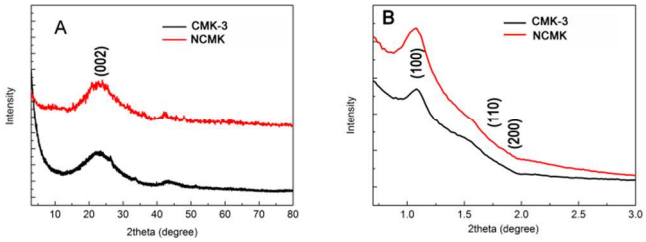

Fig. 2 Wide (A) and low angle (B) XRD patterns of CMK-3 and NCMK

To further study the porous structure and pore-size distribution of the as–obtained products, nitrogen adsorption-desorption isotherms were carried out. As shown in **Fig. 3**A, both the isotherms of CMK-3 and NCMK can be classified as type IV. In a low relative pressure range (below < 0.4), the isotherm exhibits a linear absorption. However, hysteresis loops for both samples can be observed in the relative pressure range of P/P_0 (0.4–0.8), indicating the existence of abundant uniform mesoporous structures. The BET specific surface area (SSA) of CMK-3 is 1404.8 m^2g^{-1}, while that of NCMK is only about 844.7 m^2g^{-1}. The pore-size distribution was determined by Barrett–Joyner–Halenda (BJH) method from the desorption branch of the isotherm. As shown in **Fig. 3**B, it can be seen that CMK-3 and NCMK samples exhibit a uniform pore size distribution centered at about 3.7 nm and 4.9 nm, respectively. This experiment indicated that the pore width of ordered mesoporous carbon can be enlarged by urea treatment, similar to the previous report by Weinberger *et al*.[28] The mechanism of enlarging pore width of mesoporous carbon for urea is still not very clear, which might be related to reaction of urea with carbon during heat-treatment. [29] As is known, urea will decompose into gases like NH_3.[30] It is supposed that these released gas reacted with carbon, leading to the doping of N and the increased pore width. The BET SSA decreased due to the increase of pore width, which is similar to previous reports. [30, 31]

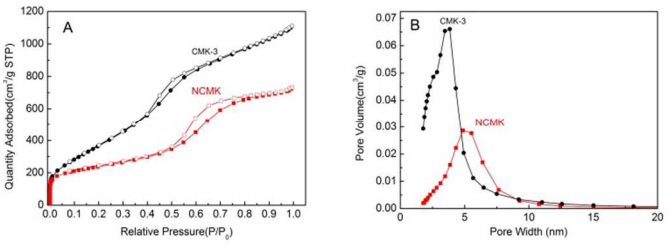

Fig. 3 (A) Isotherm of CMK-3 and NCMK; (B) Pore width distribution using BJH model (desorption branch)

The XPS measurement was carried out to study the chemical composition of NCMK. As shown in the survey XPS spectrum of the NCMK sample (**Fig. 4**A), two peaks at about 284.8 and 399.7 eV are clearly visible, corresponding to the C1s and N1s elements, respectively, indicating the presence of N element. The doping amount of N element to as prepared sample is ~ 6.2 % (atomic ratio) based on the XPS experiment. **Fig. 4**B shows the deconvolutions of the high resolution N1s spectrum to identify the surface functionalities. The N1s peak can be fitted by four component peaks at 398.2, 399.4, 401 and 403.2 eV, which can be attributed to pyridinic (N–6), pyrrolic/pyridine (N–5), quaternary nitrogen (N–Q) and pyridine N-oxygen (N–X), respectively. Among these N functionalities, the amounts of pyridinic and quaternary nitrogen are dominant because the pyrrolic nitrogen has a tendency to transform into pyridinic and quaternary ones at high temperature (above 800 °C). [29] Notably, the presence of pyridinic and quaternary structures helps to improve the electrochemical performance, especially for rate performance and conductivity.[20, 30]

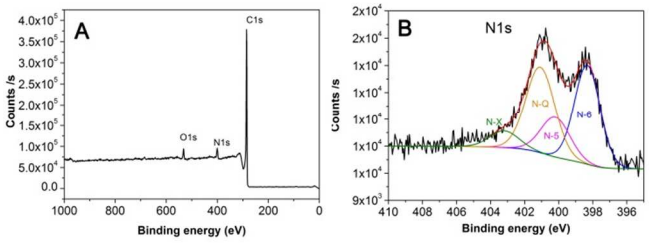

Fig. 4 Survey spectrum (A) and high resolution N1s spectrum (B) of NCMK

The electrochemical behaviour of the as-prepared mesoporous carbon was studied by CV analysis (shown in **Fig 5).** In the first scan for CMK-3 electrode, an intense irreversible peak occurs around 0.35 V, which is related to the formation of a solid electrolyte interface (SEI) layer on the surface of electrode due to the decomposition of the electrolyte.[32] Due to the decomposition, the integral area of the first scan is much larger than that of second scan. For second scan, the CV curve shows good repeatability, indicating the high reversibility of the subsequent reactions. This large irreversible capacity can be attenuated by optimizing electrolyte ingredient, and/or using SEI–forming additives. [33-35] The broad reduction/oxidation range is attributed to the mechanism of sodium insertion/removal in a wide potential range. [36]

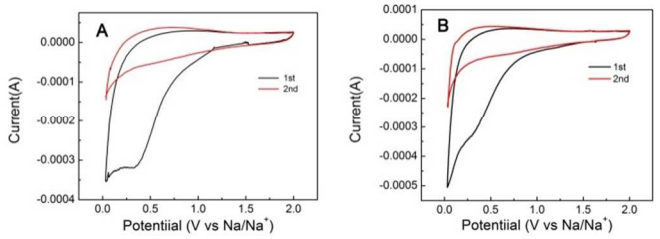

Fig. 5 CV curves of CMK-3 (A) and NCMK (B) at scan rate of 0.1mV/s.

Judging from the curve shape of the first cycle for CMK-3 and NCMK electrodes, their reaction mechanisms in SIB are somehow different. The differences in their mechanisms might be related to the differences in the local structure and the doping nature. [14,37]

Fig. 6A displays the typical charge and discharge curves of NCMK electrodes at varied current density from 0.005 to 2V, presenting a long sloping curve with no obvious plateau. According to previous studies, the mechanism of sodium storage for as prepared samples can be assigned to reversible binding of Na at graphene divacancies and StoneWales defects between graphene layers because no obvious plateau can be seen in the dominant sloping profile of discharge curve. [11, 12, 37] It has been proposed that the mechanism of sodium insertion of nanopores or insertion between graphene layers will lead to a voltage plateau at low potential below 0.1 V vs Na/Na^+.[23,37]

As shown in **Fig. 6**B, the NCMK electrode can deliver as high as 259 mAh g^{-1} at 0.2 A g^{-1}, in contrast the pure CMK-3 electrode can deliver a capacity about 170 mAh g^{-1} at the same rate. Even at higher current density, the NCMK electrode exhibit fair electrochemical performance. The NCMK electrode can deliver a discharge capacity of 203 mAh g^{-1} at 0.5 Ag^{-1}, 157 mAh g^{-1} at 1 Ag^{-1} and 98 $mAhg^{-1}$ at 2 Ag^{-1}, showing the good rate performance. The discharge capacity is higher or close to those recently reported values of expanded graphite (91 mAh g^{-1} at 0.2 Ag^{-1}),[38] templated carbon(130 $mAhg^{-1}$ at 74.4 mAg^{-1}), hollow carbon nanowire (149 mAh g^{-1} at 0.5 A g^{-1}),[23] carbon nanofiber (136 mAh g^{-1} at 0.5 A g^{-1})[36], N-doped carbon fibre (153 mAh g^{-1} at 1 Ag^{-1})[20] and carbon nanosheets framework. (106 mAh g^{-1} at 2 Ag^{-1}).

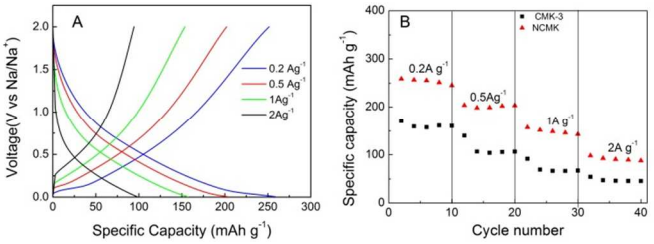

Fig. 6. (A) Charge-discharge curve of NCMK electrode at varied current density; (B) Rate performance test for NCMK. (The cell was pre-cycled at 100 mA g^{-1} for 10 cycles before the rate performance)

Fig. 7A showed the cycle performance of NCMK and CMK-3 electrodes at current density of 0.1 Ag^{-1}. The NCMK electrode can deliver a specific capacity of 374.3 $mAhg^{-1}$ for the first discharge, which is much large than that (246.1 $mAhg^{-1}$) of CMK-3. At the 45th cycle, the NCMK can still deliver a specific capacity of 327.6 mA h g^{-1}, in contrast CMK-3 deliver that of 217.7 mA h g^{-1}. The fade rate for NCMK and CMK-3 is only 1.06 and 0.65 mAh g^{-1} per cycle, respectively, indicating the good cycle performance.

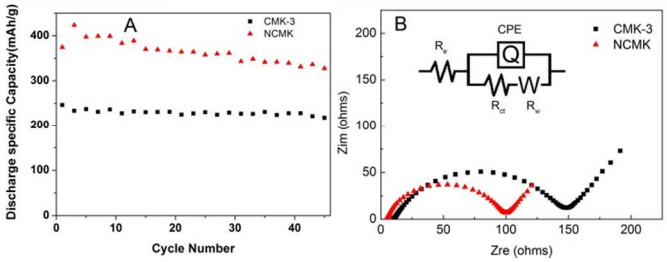

Fig. 7 (A) Cycle performance of CMK-3 and NCMK electrodes at current density of 100 mA g^{-1} (The cell was pre-cycled at 50 mA g^{-1} for 5 cycles before the cycle performance); (B) Nyquist plots of CMK-3 and NCMK electrodes (inset, equivalent circuit).

On hand, the ordered mesopores not only act as the fast pathways of ion transport but also decrease the diffusion length of ion, leading to improved electrochemical performance.[39] On the other hand, the nitrogen doping can further enhance the performance due to the presence of pyridinic and quaternary structure.[20,26,30] Furthermore, the local structure for NCMK has become more disordered during N-doping process, and the disordered structure is favourable to the storage of sodium. [14] In all, the improved performance for as prepared N-doped OMC can be attributed to the more disordered local structure, the doping of nitrogen and the mesoporous pathway for sodium ions.

An equivalent circuit model was constructed to analyze the impedance spectra, shown in inset of **Fig. 7B**. An intercept with X axis in high frequency corresponded to the ohmic resistance (*R*e), which represented the resistance of the electrolyte. The semicircle in the middle frequency range was related to the charge transfer resistance (*R*ct). The inclined line in the low frequency represented the Warburg impedance (*Z*w), which was associated with Na-ion diffusion in the electrodes. A constant phase element CPE represents the double layer capacitance and passivation film capacitance. Rct was estimated ca. 90.0 and 130.7 ohms calculated according to Zsimwin software for CMK-3 and NCMK electrodes, respectively. The lowered resistance for NCMK is probably attributed to more rapid transport within the enlarged width and the improved conductivity due to the introduced heteroatom.

Conclusion

For the first time, the electrochemical performance of N-doped OMCs as anode in SIB was studied, in which N-doped OMC was prepared via a template method. During the preparation process, urea not only performs as a source of N-doping but also has a substantial effect on modifying the pore width and the local structure for as prepared OMCs. N-doped OMC was found to have good performance in capacity as well as rate capability at room temperature as disclosed by electrochemical experiments. The improved electrochemical performance of NCMK is attributed to the synergetic effect of the more disordered local structure, N-doping nature and the mesoporous pathway. Considering the diverse structures of OMCs (such as hexagonal and cubic structures), various doping elements (such as N, S and B elements) available and doping level variable, the OMCs such as N-doped OMC in this work are very promising in SIB in future.

Acknowledge:

This work was financially supported by NSFC (Grant No.51202212, 21107117), Natural Science Foundation of Hebei province (Grant No. E2014203033), Beijing Natural Science Foundation (Grant No. 2132057).

Notes and references

[a] State Key Laboratory of Metastable Materials Science and Technology, College of Materials Science and Engineering, Yanshan University, Qinhuangdao, Hebei Province, 066004, China. E-mail: liyueming@ysu.edu.cn.

[b] Key Laboratory of Photochemical Conversion and Optoelectronic Materials and HKU-CAS Joint Laboratory on New Materials, Technical Institute of Physics and Chemistry, Chinese Academy of Sciences, Beijing 100190, China. E-mail:xjlv@mail.ipc.ac.cn

1. S. P. Ong, V. L. Chevrier, G. Hautier, A. Jain, C. Moore, S. Kim, X. Ma and G. Ceder, *Energy Environ. Sci*, 2011, **4**, 3680-3688.
2. S. Bose, T. Kuila, A. K. Mishra, R. Rajasekar, N. H. Kim and J. H. Lee, *J. Mater. Chem.*, 2012, **22**, 767-784.
3. P. Senguttuvan, G. Rousse, V. Seznec, J.-M. Tarascon and M. R. Palacín, *Chem. Mater.*, 2011, **23**, 4109-4111.
4. M. Shirpour, J. Cabana and M. Doeff, *Energy Environ. Sci.*, 2013, **6**, 2538-2547.
5. Y. Xu, Y. Zhu, Y. Liu and C. Wang, *Adv. Energy Mater.*, 2013, **3**, 128-133.
6. M. K. Datta, R. Epur, P. Saha, K. Kadakia, S. K. Park and P. N. Kumta, *J. Power Sources*, 2013, **225**, 316-322.
7. A. Darwiche, C. Marino, M. T. Sougrati, B. Fraisse, L. Stievano and L. Monconduit, *JACS*, 2012, **134**, 20805-20811.
8. S.-W. Kim, D.-H. Seo, X. Ma, G. Ceder and K. Kang, *Adv. Energy Mater.*, 2012, **2**, 710-721.
9. B. L. Ellis and L. F. Nazar, *Curr Opin. Solid State Mater. Sci.*, 2012, **16**, 168-177.
10. Z. Wang, S. M. Selbach and T. Grande, *RSC Adv.*, 2014, **4**, 4069-4079.
11. D. A. Stevens and J. R. Dahn, *J. Electrochem. Soc.*, 2001, **148**, A803-A811.
12. D. Datta, J. Li and V. B. Shenoy, *ACS Appl. Mater. Interf.*, 2014, **6**, 1788-1795.
13. C. Ling and F. Mizuno, *Phys.Chem.Chem.Phys.*, 2014, **16**, 10419-10424.
14. Y. Liu, F. Fan, J. Wang, Y. Liu, H. Chen, K. L. Jungjohann, Y. Xu, Y. Zhu, D. Bigio, T. Zhu and C. Wang, *Nano Lett.* , 2014, **14**, 3445-3452.
15. J. Ding, H. Wang, Z. Li, A. Kohandehghan, K. Cui, Z. Xu, B. Zahiri, X. Tan, E. M. Lotfabad, B. C. Olsen and D. Mitlin, *ACS Nano*, 2013, **7**, 11004-11015.
16. S. Wenzel, T. Hara, J. Janek and P. Adelhelm, *Energy Environ. Sci.*, 2011, **4**, 3342-3345.
17. R. Ryoo, S. H. Joo, M. Kruk and M. Jaroniec, *Adv. Mater.*, 2001, **13**, 677-681.
18. J. Wei, D. Zhou, Z. Sun, Y. Deng, Y. Xia and D. Zhao, *Adv. Funct. Mater.*, 2013, **23**, 2322-2328.
19. J. Cao, Y. Wang, Y. Zhou, J.-H. Ouyang, D. Jia and L. Guo, *J. Electroanal. Chem.*, 2013, **689**, 201-206.
20. L. Fu, K. Tang, K. Song, P. A. van Aken, Y. Yu and J. Maier, *Nanoscale*, 2014, **6**, 1384-1389.
21. W. H. Shin, H. M. Jeong, B. G. Kim, J. K. Kang and J. W. Choi, *Nano Lett.*, 2012, **12**, 2283-2288.
22. Y. Wu, S. Fang and Y. Jiang, *J. Mater. Chem.*, 1998, **8**, 2223-2227.
23. Y. Cao, L. Xiao, M. L. Sushko, W. Wang, B. Schwenzer, J. Xiao, Z. Nie, L. V. Saraf, Z. Yang and J. Liu, *Nano Lett*, 2012, **12**, 3783-3787.
24. H.-g. Wang, Z. Wu, F.-l. Meng, D.-l. Ma, X.-l. Huang, L.-m. Wang and X.-b. Zhang, *Chemsuschem*, 2013, **6**, 56-60.
25. Z. Wang, L. Qie, L. Yuan, W. Zhang, X. Hu and Y. Huang, *Carbon*, 2013, **55**, 328-334.
26. Y. Li, Z. Wang and X.-J. Lv, *J. Mater. Chemi. A*, 2014, **2,** 15473-15479
27. S. Jun, S. H. Joo, R. Ryoo, M. Kruk, M. Jaroniec, Z. Liu, T. Ohsuna and O. Terasaki, *JACS*, 2000, **122**, 10712-10713.
28. C. Weinberger, S. Haffer, T. Wagner and M. Tiemann, *European J. Inorg. Chem.*, 2014, **2014**, 2787-2792.
29. M. Florent, M. Tocci and T. J. Bandosz, *Carbon*, 2013, **63**, 283-293.

30. M. Seredych, D. Hulicova-Jurcakova, G. Q. Lu and T. J. Bandosz, *Carbon*, 2008, **46**, 1475-1488.
31. K. Xia, Q. Gao, J. Jiang and J. Hu, *Carbon*, 2008, **46**, 1718-1726.
32. K. Tang, L. Fu, R. J. White, L. Yu, M.-M. Titirici, M. Antonietti and J. Maier, *Adv.Energy Mater.*, 2012, **2**, 873-877.
33. Y. Matsumura, S. Wang and J. Mondori, *J. Electrochem. Soc.*, 1995, **142**, 2914-291832.
34. Z.-S. Wu, W. Ren, L. Xu, F. Li and H.-M. Cheng, ACS Nano, 2011, 5, 5463-5471.
35. S.-K. Jeong, M. Inaba, R. Mogi, Y. Iriyama, T. Abe and Z. Ogumi, *Langmuir*, 2001, **17**, 8281-8286.
36. T. Chen, Y. Liu, L. Pan, T. Lu, Y. Yao, Z. Sun, D. H. C. Chua and Q. Chen, *J. Mater Chem A,* 2014, **2**, 4117-4121.
37. E. M. Lotfabad, J. Ding, K. Cui, A. Kohandehghan, W. P. Kalisvaart, M. Hazelton and D. Mitlin, *ACS Nano*, 2014, **8**, 7115-7129.
38. Y. Wen, K. He, Y. Zhu, F. Han, Y. Xu, I. Matsuda, Y. Ishii, J. Cumings and C. Wang, *Nat Commun*, 2014, **5**, doi:10.1038/ncomms5033
39. H. Zhou, S. Zhu, M. Hibino, I. Honma and M. Ichihara, *Adv. Mater.*, 2003, 15, 2107-2111.